International Journal of Pharmaceutics 685 (2025) 126290

Contents lists available at ScienceDirect

International Journal of Pharmaceutics

journal homepage: www.elsevier.com/locate/ijpharm

Exploring a mucoacting spray-dried nanoparticle-in-microparticle inhalable formulation for targeted pulmonary delivery of sorafenib in lung cancer therapy

Cinzia Scialabba, Federico Corsaro, Salvatore Emanuele Drago, Emanuela Fabiola Craparo *, Gennara Cavallaro

Lab of Biocompatible Polymers, Department of Biological, Chemical and Pharmaceutical Sciences and Technologies (STEBICEF), University of Palermo, Via Archirafi 32, Palermo 90123, Italy

ARTICLE INFO

Keywords:
Cancer
Sorafenib
Nanoparticles
Active targeting
Nano into micro

ABSTRACT

In this study, we developed an inhalable Nano–in–Micro (NiM) system for localized delivery of Sorafenib (Sor) in non-small cell lung cancer (NSCLC) therapy. Sor was encapsulated into mucus-penetrating and folate-targeted polymeric nanoparticles (FA-PPP-NPs@Sor), produced starting from the α,β-poly(N-2-hydroxyethyl)-D,L-aspartamide (PHEA), functionalised with poly(lactic-*co*-glycolic acid) (PLGA), and folate-conjugated polyethylene glycol (PEG-FA) FA ($DD_{PLGA} = 3.3$ mol %, $DD_{PEG–FA} \approx 8$ chains/molecule). Nanoprecipitation produced 109 nm particles, easy to redisperse, with a DL of 10 wt%, which showed a controlled release of the drug, about 8.4 wt% (pH 7.4) vs. 21.7 wt% (pH 5.5) in 24 h. A selective cytotoxicity towards A549 lung cancer cells via folate receptor-mediated internalization was found, being $IC_{50} = 18 \pm 3.2$ μM, significantly lower than those found both in 16HBE cells ($IC_{50} = 69 \pm 3.1$ μM and free Sor ($IC_{50} = 17.7 \pm 2.3$ μM). The receptor involvement was confirmed by competitive folate blocking, which raised IC_{50} >100 μM. Wound healing assay performed to evaluate the ability of Sor-loaded nanoparticles to inhibit or reduce cell migration showed 27 % vs. 40 % wound closure at 48 h (NiM vs Sor). The nanoparticles were further incorporated into inhalable microparticles via spray drying (SD), using mannitol, leucine, N-acetylcysteine, and ammonium bicarbonate as functional excipients (yield 63 wt%, EE = 100 wt%, DL = 0.35 wt%). The spray dried NiM_{Sor} microparticles exhibited a MMAD and a FPF, respectively, of 2.2 μm and 76 %, suitable for deep lung delivery. Furthermore, their storage at r.t. and dissolution in water reconstitutes the nanoparticle dispersion. Rheology tests demonstrated time– and concentration–dependent mucus thinning. Overall, this study presents a promising inhalable platform for targeted lung cancer therapy, combining targeted cytotoxicity, mucus penetration, controlled release, and favourable aerosol properties.

1. Introduction

Lung cancer is one of the most prevalent malignancies worldwide (Naccache et al., 2018; Sung et al., 2021). It is broadly categorized into two major histological subtypes: non-small cell lung cancer (NSCLC) for approximately 85 % of cases, and the more aggressive form small cell lung cancer (SCLC) for the remaining 15 % (Duruisseaux and Esteller, 2018).

Despite advances in early detection through imaging techniques, lung cancer is often diagnosed at an advanced stage due to its asymptomatic nature in the early phases. As a result, the prognosis remains poor, although this varies significantly based on the cancer stage at diagnosis and treatment. Conventional systemic chemotherapy, given by parenteral administration, is associated with low drug accumulation in the tumor site, high toxicity and adverse reactions, suboptimal clinical outcomes, and reduced patient survival rates. Similarly, immunotherapeutic strategies may induce autoimmune manifestations and vascular leak syndrome, thus posing significant safety challenges (Wang et al., 2021).

Given the significant drawbacks associated with both conventional treatments and parenteral administration route, there is a growing interest in innovative approaches to treat lung cancer. Among these, the

* Corresponding author.
E-mail address: emanuela.craparo@unipa.it (E.F. Craparo).

https://doi.org/10.1016/j.ijpharm.2025.126290
Received 25 July 2025; Received in revised form 13 October 2025; Accepted 14 October 2025
Available online 17 October 2025

use of inhalable formulations is a promising strategy, as they allow a direct lung deposition of the drug, that is associated to a rapid onset of action while bypassing first-pass metabolism, reduction of systemic exposure and adverse off-site effects. Additionally, inhalation is a non-invasive and patient-friendly method, improving adherence (Kim et al., 2012).

However, direct drug inhalation in the respiratory tract also presents significant challenges due to the presence of several physiological barriers, including mucociliary clearance, a mucus layer, and the activity of alveolar macrophages, which could significantly limit the effective deposition, penetration, and retention of therapeutic agents.

In this context, nanoparticle-based drug delivery systems (NDDS) have gained considerable attention for inhalation therapy, offering significant advantages over traditional drugs in the treatment of lung cancer, such as improvement of drug stability, prolonged drug release and retention time in the lungs, and reduction of off-target toxicity compared to conventional formulations. Moreover, thanks to their nanometric size and the possibility of surface decoration with muco-penetrating polymers and/or targeting ligands, these carriers could overcome the mucosal barriers, enhance drug penetration and targeting directly to lung cancer cells, increasing therapeutic efficacy and reducing side effects on healthy tissue (Triolo et al., 2017). Since nanoparticles are not suitable for inhalation due to nanometric size, their embedding into microparticles with aerodynamic properties suitable for efficient deposition in the deep lung regions has emerged as a cutting-edge nano into micro (NIM) strategy for efficient pulmonary drug delivery (Craparo et al., 2024; Scialabba et al., 2024).

Sorafenib is the chemotherapeutic agent currently approved for parenteral administration in the treatment of liver and pancreatic cancers (Kutkowska et al., 2017; Wang et al., 2019). Its mechanism of action involves inhibiting tumour cell proliferation, promoting apoptosis, and suppressing angiogenesis (Craparo et al., 2014; Hendrixson et al., 2024). Several studies have already proved its potential repositioning as a second and third-line treatment for lung cancer (Blumenschein et al., 2009; Takezawa et al., 2009; Zhang et al., 2012). However, its clinical effectiveness is limited by poor solubility and low bioavailability. Therefore, to address these limitations, encapsulating Sorafenib in nanocarriers has emerged as a promising strategy to improve lung bioavailability by inhalation (Abdellatif et al., 2022; Shukla et al., 2020; Su et al., 2018). Shukla S. et al. have described an innovative inhalable formulation based on polymeric nanocarriers loaded with Sorafenib for the treatment of NSCLC, as promising alternative to conventional parenteral administration (Shukla et al., 2020). Another noteworthy contribution comes from Asghar Narmani et al., who described the development of smart nanocarriers based on chitosan-PLGA polymers, functionalized with folic acid (FA) as a ligand to specifically bind to folate receptors, that are overexpressed on the surface of lung cancer cells. By the receptor-mediated endocytosis, this method enhanced the selective uptake of nanoparticles by tumour cells, thereby improving therapeutic efficacy while reducing systemic side effects (Narmani et al., 2023).

Keeping in mind this scenario, in this study, we described an advanced inhalable drug delivery system based on polymeric nanoparticles, which were obtained by using a biocompatible graft copolymer of α,β-poly(N-2-hydroxyethyl)-D,L-aspartamide (PHEA) and poly (lactic-co-glycolic acid) (PLGA), to enable controlled and sustained drug release. Polyethylene glycol (PEG) was used to impart stealth characteristics, helping potentially the system to escape immune recognition and prolong its retention in the pulmonary environment (Craparo et al., 2024). Moreover, FA exposed on the nanoparticle surface using PEG chain spacers was used to enhance drug accumulation into tumor cells after inhalation (Iwakiri et al., 2008; Puleio et al., 2020).

To allow the deposition into the deep lungs, a Nano-into-Micro (NiM) approach was followed, embedding these nanoparticles within inhalable microparticles using a spray-drying (SD) process (Craparo et al., 2024). This technique enables precise control over particle size and aerodynamic properties, ensuring efficient lung deposition. To enhance dispersibility, mucus penetration, and particle dissolution, the formulations were tailored using functional excipients such as mannitol (MAN), leucine (LEU), N-acetylcysteine (NAC), and the porogen agent ammonium bicarbonate (AB) (Abdelaziz et al., 2018; Lababidi et al., 2020; Mancini et al., 2023).

2. Experimental section

2.1. Materials and methods

Anhydrous N, N'-dimethylformamide (DMF-a), anhydrous N, N'-dimethylacetamide (DMA-a), folic acid (FA), poly(lactic-*co*-glycolic acid) (PLGA acid-free, $\overline{M}_w$) 10,000–12,000 Da), deuterium oxid (D_2O) deuterated N, N'-dimethylformamide (DMF-d_7), bis-aminopolyethylene $glycol_{2000}$ (NH_2-PEG-NH_2, $\overline{M}_w$) = 2,000 Da), diethylamine (DEA), triethylamine (TEA), 1,1′-carbonyldiimidazole (CDI), disuccinimidyl carbonate (DSC), polyvinyl pyrrolidone 40 KDa (PVP), sorafenib (Sor), diethyl ether, acetone, ethanol, acetonitrile (ACN), dichloromethane (DCM), mucin from porcine stomach, Dulbecco's phosphate-buffered saline (DPBS), D-mannitol (MAN), leucin (LEU), N-acetyl cysteine (NAC), ammonium bicarbonate (AB) and polystyrene standards (10,000–150,000 Da), were purchased from Sigma-Aldrich (Italy). Dialysis membranes were purchased from Spectrum Labs (USA). All reagents used were of analytical grade. Human lung cancer cells (A549) and human bronchial epithelial cells (16HBE) were sourced from Clini-Sciences (Guidonia Montecelio, Italy).

^{1}H NMR spectra were acquired using a Bruker Avance II300 spectrometer operating at 300 MHz.

Size exclusion chromatography (SEC) analysis was carried out using a Phenomenex Phenogel 5u •10^4 column (California, USA) connected to an Agilent 1260 Infinity Multi-Detector GPC/SEC system with refractive index (RI) detection, and at 90° and 15° light scattering (LS) detection. The mobile phase was DMF containing 0.1 % w/v LiBr and flow rate of 0.8 mL/min, the column temperature was maintained at 50 °C. Each sample (15 mg/mL) were solubilized in the mobile phase and filtered with 0.2 μm pore size filter before injecting. Calibration curve for determining the relative weight average molecular weight ($\overline{M}_w$) was obtained using polystyrene standards (10,000–150,000 g/mol), while for absolute $\overline{M}_w$ a 80,000 g/mol polystyrene standard was employed.

Preparation and purification of α,β-poly(N-2-hydroxyethyl)-D,L-aspartamide (PHEA) and PHEA-*g*-PLGA graft copolymer followed previously established methods (Scialabba et al., 2024).

2.2. Synthesis of folate-amino polyethylene $glycol_{2000}$ (H_2N-PEG-FA)

Derivatization of H_2N-PEG-NH_2 with folic acid (FA) was performed using CDI as a coupling agent to activate the carboxyl group of FA. In detail, 74 mg of CDI were added to 100 mg of FA previously dispersed in 6 ml of DMSO-a. The resulting dispersion was left to react at 40 °C under an inert atmosphere for 3 h. Simultaneously, a solution of H_2N-PEG-NH_2 was prepared by dissolving the polymer in DMSO-a at a concentration of 113 mg/mL, using DEA as a catalyst agent. After activation, the H_2N-PEG-NH_2 solution slowly was added drop by drop to the FA solution. The reaction mixture was allowed to react, under an inert atmosphere under continuous stirring at 40 °C for 20 h. The obtained product was purified by exhaustive dialysis using a membrane with nominal molecular weight cutoff (MWCO) of 2 KDa against distilled water adjusted with NaOH to pH 9, to remove the organic solvent, unreacted CDI and FA. The dialyzed dispersion was then freeze-dried, yielding a yellow powder. This powder was redissolved in 2 ml of distilled water and further purified by gel permeation chromatography (GPC) using Sephadex G-25 as stationary phase. The stoichiometric ratios employed were: moles of CDI/moles of FA = 2, moles of FA/moles of H_2N-PEG-NH_2 = 2 and moles

of DEA/moles of H_2N-PEG-NH_2 = 0.75.

The final yield was 44.5 % w/w calculated based on the initial weight of NH_2-PEG-NH_2. H_2N-PEG-FA was characterized by ^1H NMR analysis in D_2O. The ^1H NMR spectrum (300 MHz, 25 °C, TMS) showed the following peaks: a δ 3.1–3.6 ($2H_{PEG}$, $-[CH_2\mathbf{CH_2}O]_{44}$-); δ 6.6 (2 H_{FA} −[C(O)-C-**CH**=CH]-; δ 7.5 (2 H_{FA} −[NH-C-**CH**=CH]-); δ 8.5 (1 H_{FA} −[C-**CH**=N]-).

2.3. Synthesis of PHEA-g-PLGA-g-PEG-FA

The functionalization of PHEA-*g*-PLGA (Craparo et al., 2024) with H_2N-PEG-FA was performed in DMA-a using DSC as coupling agent and TEA as a catalyst, according to the following stoichiometric conditions: moles of DSC/moles of repeat unit of PHEA = 0.1 and moles of TEA/moles of DSC = 1. Specifically, to a dispersion of PHEA-*g*- PLGA in DMA-a (50 mg/mL) a proper amount of DSC and TEA were added, and the mixture stirred at 40 °C for 4 h to activate the hydroxyl groups of PHEA repeating unit. Meanwhile, a solution of H_2N-PEG-FA in DMA-a (17 mg/mL) was prepared, based on a molar ratio of 0.075 mol of H_2N-PEG-FA per mol of PHEA repeating unit. After the activation period, the of PHEA-*g*- PLGA dispersion was added dropwise to the H_2N-PEG-FA dispersion under stirring.

The reaction mixture was then maintained at 25 °C for 24 h. Following this step, the reaction mixture was placed in a dialysis tube, using a membrane with MWCO of 25 kDa against distilled water, to remove the organic solvent and the unreacted H_2N-PEG-FA. The final product was recovered by freeze-drying and the yield was found to be equal to 75 % w/w compared to the starting PHEA-*g*-PLGA weight. PHEA-*g*-PLGA-*g*-PEG-FA was characterized by ^1H NMR analysis. The ^1H NMR spectrum in DMF d_7 (300 MHz, 25 °C, TMS) highlighted the following peaks: δ 1.5–1.9 ($3H_{PLGA}$,-[OCO-CH(C**H**$_3$)]$_{92}$-); δ 3.0 ($2H_{PHEA}$, –COCHC**H**$_2$CONH-); δ 3.5 ($2H_{PHEA}$, –NHC**H**$_2$CH$_2$O-); δ 3.6 ($2H_{PHEA}$, –NHCH$_2$C**H**$_2$O-); δ 3.7 ($4H_{PEG}$, $-[CH_2C\mathbf{H}_2O]_{44}$-); δ 5.0 ($1H_{PHEA}$, –NHC**H**(CO)CH$_2$–); δ 4.2–4.5 e 5.4–5.8 ($1H_{PLGA}$, $-[OCOC\mathbf{H}(CH_3)]_{92}$-); δ 5.3 ($2H_{PLGA}$, $-[OCOC\mathbf{H}_2]_{92}$).

2.4. Production of PHEA-g-PLGA-g-PEG-FA nanoparticles (FA-PPP-NPs)

Empty (FA-PPP-NPs) and Sor-loaded nanoparticles (FA-PPP-NPs@Sor) were obtained through the nanoprecipitation method (Craparo et al., 2022b). In detail, 50 mg of PHEA-*g*-PLGA-*g*-PEG-FA and 10 mg of Sorafenib (Sor) were dissolved in 2 ml of DMSO and added dropwise under stirring to 20 ml of PVP dispersion (0,4% w/v). The obtained nanoparticles were purified by exhaustive dialysis, using a membrane with MWCO of 12–14 kDa, to remove DMSO solvent, and after six hours moved to 100 kDa dialysis overnight to remove the excess of PVP. Finally, unloaded Sor was removed by filtration using a 5 μm regenerated cellulose (RC) syringe filter. Moreover, FA-PPP-NPs and unpegylated nanoparticles (PP-NPs) were prepared as control samples using the same procedure.

2.5. Characterization of nanoparticles

2.5.1. Dimensional analysis and ζ-potential measurements

The average size (nm), polydispersity index (PDI), and **ζ**-potential values of each sample were determined on water nanoparticle dispersions (1 mg/mL) by Dynamic light scattering (DLS) using a Malvern Zetasizer NanoZS (Malvern Instruments, Worcestershire, U.K.). In particular, the measurements were carried out with a fixed angle of 173° at a temperature of 25 °C. The **ζ**-potential values (mV) were calculated from electrophoretic mobility using the Smoluchowski relationship. Each nanoparticle dispersion was analyzed in triplicate.

2.5.2. Measurement of interactions with mucin

The interaction between mucin and each nanoparticle sample (FA-PPP-NPs or FA-PPP-NPs@Sor) was evaluated by using turbidimetry (Craparo et al., 2022a). The experiment was conducted by dispersing both nanoparticles' samples and mucin in PBS at pH 7.4 at a concentration of 2 mg/mL. Then, these dispersions were mixed in a 1:1 v/v ratio obtaining a final nanoparticles e mucin concentration of 1 mg/mL. Following incubation at 37 °C, turbidity was assessed by measuring transmittance at 650 nm at time 0 and after 30 min and 1, 2, and 3 h. The absorbance of mucin and nanoparticles dispersed in PBS at pH 7.4 was also evaluated as control. All measurements were conducted in triplicate. As a control, the same procedure was applied to unpegylated nanoparticles made of PHEA-*g*-PLGA graft copolymer (PP-NPs).

2.5.3. Determination of drug loading (DL%) and encapsulation efficiency (EE%)

The amount of Sor encapsulated into the FA-PPP-NPs was determined by high-performance liquid chromatography (HPLC) analysis using a method reported elsewhere (Craparo et al., 2014). Briefly, an Agilent 1260 Infinity II equipped with an autosampler (100 μL injection volume) and a 1260 VWD UV–Vis HPLC detector was used with a C6-phenyl column (250 × 4.6 mm, Phenomenex) and a mobile phase consisting of a mixture of methanol and bidistilled water (85:15 v/v) operating with a flow rate of 1 ml/min. The analysis was performed in isocratic conditions at 25 °C and the absorbance of Sor was detected at 207 nm. Samples were prepared dispersing a known quantity of PPP-FA-NPs@Sor sample in 100 μL of DMSO and stirred for 30 min. Then, 900 μL of the mobile phase was added. Before injection into the column, the samples were filtered using 0.22 μm RC syringe filters. The amount of loaded drug into nanoparticles, expressed as drug loading % (DL%), was calculated by using a calibration curve obtained from different concentration of Sor used as standard.

2.5.4. Release studies

The release of Sor from FA-PPP-NPs@Sor was determined in two different release media: simulated lung fluid at pH 7.4 (SLF4) (Marques et al., 2011) and in citrate buffer at pH 5.5, both supplemented with fetal bovine serum (FBS) at 50 % v/v, using the dialysis method. Briefly, 5 mg of FA-PPP-NPs@Sor were dispersed in 2.5 ml of each medium without FBS and transferred inside the dialysis membrane tube (MWCO of 12,000 Da). This dialysis membrane was immersed in 22.5 ml of external release media and incubated under continuous stirring (100 rpm) in an orbital shaker at 37 °C. At predetermined time points (0, 1, 2, 4, 6, 8, and 24 h) aliquots of external medium (1 ml) were withdraw from outside of membrane dialysis and replaced with equivalent volume of fresh medium.

Each collected medium was mixed with 4 ml of MeOH, and after 1 h filtered through a 0.22 μm RC syringe filter and analyzed by HPLC under the previously described conditions. Each experiment was carried out in triplicate and the results agreed within ± 5 % standard error.

2.6. Biological characterization

The biological characterization of empty and FA-PPP-NPs@Sor was carried out on human lung cancer cells (A549), on two different human epithelial bronchial cells (16HBE). The cells were cultured in flasks at 37 °C under a humidified atmosphere containing 5 % CO_2. The growth medium consisted of Minimum Essential Medium (MEM) (Costar, Corning, MA, USA), supplemented with 10 % fetal bovine serum (FBS), 1 % L-glutamine, and 1 % penicillin/streptomycin (all obtained from Euroclone).

2.6.1. Cell cytotoxicity

The cytotoxic effects of free Sor, FA-PPP-NPs, and FA-PPP-NPs@Sor were evaluated in vitro on A549 and 16HBE cell lines using the tetrazolium salt (MTS) assay. Cells were seeded into 96 multiwell plates at density of 5×10^3 cells per well and grown in DMEM. After 24 h, the medium was replaced with 200 μl of fresh DMEM containing FA-PPP-NPs and FA-PPP-NPs@Sor at various concentrations, corresponding to

equivalent concentration of Sor ranging from 10 to 100 mM. Following 24 and 48 h of incubation, MTS assay was performed according to the manufacturer's instructions. Free Sor dispersions, prepared by diluting a DMSO stock solution (1 mg/mL) into DMEM, were used as positive control. Untreated cells were used as negative control. Cell viability was expressed as a percentage relative to the absorbance of the untreated control group, which was set at 100 % viability. An additional cytotoxicity assay was conducted on A549 cells to evaluate the competitive effect of folic acid. Cells were pre-treated with a FA solution (100 μg/ml) for 4 h prior to incubation with either free sorafenib or FA-PPP-NPs@Sor under the same experimental conditions. All experiments were performed in triplicate, and results were expressed as mean ± standard deviation.

2.6.2. Cell uptake study

Cell uptake was evaluated by fluorescent microscopy (Zeiss "AXIO Vert. A1″ Microscope Inverted). A549 cells were seeded at a density of 2.5×10^4 cells/well in an 8-well plate and cultured for 24 h. Subsequently, the medium was replaced with 500 μL of fresh DMEM dispersion of Rhodamine-labelled FA-PPP-NPs@Sor, corresponding to an equivalent Sor concentration of 20 μM, and cells were incubated for 4 h. After removal of the medium, the cell monolayer was washed twice with DPBS pH 7.4, fixed with 4 % formaldehyde for 10 min, and washed again with DPBS. Cell nuclei were stained with 4′,6-diamidino-2-phenylindole (DAPI) for 10 min at room temperature. Images were captured using a fluorescence microscope with an Axio Cam MRm (Zeiss). Untreated cells were used as negative control to set the auto-fluorescence.

2.6.3. Wound healing assay

The wound healing assay was performed on A549, and 16HBE cell lines to evaluate the ability of Sor loaded nanoparticles to inhibit or reduce cell migration. Cells were seeded at a density of 5×10^3 cells per well in 24-well plates and incubated overnight at 37 °C to allow the formation of a uniform monolayer. After 24 h, a linear scratch was created in each well using a sterile 200 μl pipette tip. Non-adherent and detached cells were removed by gently washing the wells twice with phosphate-buffered saline (PBS). Cells were then treated with either Sor or FA-PPP-NPs@Sor nanoparticles at concentrations of 25 μM. Wells containing cells incubated with culture medium were used as a control. Wound closure was monitored at 0 h (immediately after scratch), 24 h and 48 h. Images of the wound area were acquired using a microscope. The percentage of wound closure, indicative of cell migration, was determined by measuring the distance between the wound edges and comparing it over time.

2.7. Microparticle production and characterization

2.7.1. Preparation of spray-dried microparticles (MPs) and Nano-into-Microparticles (NiM)

MPs and NiM formulations were produced using a Mini Spray Dryer B-290 (Buchi, Milan, Italy). First, the matrix composition was properly optimized by producing an empty microparticle sample (MPs) by varying the composition of the liquid feed in terms of mannitol (MAN), leucine (LEU), N-acetyl cysteine (NAC), and ammonium bicarbonate (AB) concentration (Craparo et al., 2024). Additionally, rhodamine B (RhB) at a concentration of 0.05 % w/v was added to the liquid feed of all microparticle samples to allow fluorescence-based tracking of the particles.

In detail, MAN concentration was adjusted between 5 % and 6 % w/v, the NAC/LEU ratio was varied between 1:1 and 1:2 w/w, and the AB (porogen) content was modulated between 0.5 % and 1 % w/v. Furthermore, operating conditions, including pump flow rate and aspiration parameters were used to assess their influence on microparticle formation. The full set of MPs, as a function of the liquid feed composition and operating parameters. is reported in Table 1.

When the excipients were completely dissolved, the resulting dispersion was filtered through 5 μm syringe filters to ensure clarity and uniformity. The filtered dispersion was then spray-dried using a 140 mm atomizer nozzle, with an inlet temperature of 110 °C and an outlet temperature 60–66 °C. The dehumidified air and served as the drying gas and the pump rate were set to 10 %.

To obtain NiM particles, FA-PPP-NPs and FA-PPP-NPs@Sor were added to the liquid feed used for sample MPsF at a final concentration of 4.5 mg/mL (0.45 % w/v) prior to spray drying, obtaining NiM and NiM_{Sor} formulation. The process was carried out under the same conditions described above for the MPs. To assess the particle redispersibility and verify that SD process and 1 year storage at r.t. of NiM_{Sor} formulation did not alter their size or surface charge of the embedded nanoparticles, 15 mg of NiM were redispersed in 1 ml of bidistilled water under stirring for 15 min. Particle size, PDI, and ζ-potential were then measured via DLS.

2.7.2. Scanning electron microscopy (SEM)

The morphology of the obtained microparticle samples was analyzed using scanning electron microscopy (SEM) through a Phenom™ ProX Desktop SEM microscope (Thermo Fisher Scientific, Milan, Italy). Before recording the images, samples were fixed to a stainless-steel stub using double-sided tape. Particle size distribution and geometric diameter (d_{geom}) for each sample was obtained with the ImageJ software by analysing more than 500 particles. The theoretical aerodynamic diameter (d_{aer}) was calculated using an equation reported elsewhere (Scialabba et al., 2024).

2.7.3. Tapped density (d_{tapp})

The d_{tapp} of each powder sample was determined using the syringe method, as already reported (Craparo et al., 2024). Briefly, a known quantity of powder was introduced into a 1 ml graduated syringe, and the mass was determined by weight difference. To measure the tapped volume, the syringe was gently tapped against a flat surface from a height of 2.5 cm, repeating the motion 100 times or until the powder volume stabilized. The d_{tapp} was then calculated by dividing the powder mass by the final settled volume. All measurements were performed in triplicate.

2.7.4. Andersen cascade impactor (ACI)

The aerodynamic behavior of samples MPsF, MPsG, and NiM_{Sor} was assessed using a Handihaler® dry powder inhaler (DPI) connected to an Andersen Cascade 8 Stage Impactor (ACI, InPharmaTec) operating at an

Table 1
Qualitative-quantitative composition of the liquid feed and operating conditions to produce both empty and NiM microparticle sample by spray drying (SD).

Sample	MAN % w/v	NAC %w/v	LEU % w/v	AB % w/v	NPs % w/v	Temperature °C	Pump	Aspiration	Yield % w\w
MPsA	6	1	2	1	–	110	7	100	67.5
MPsB	6	1	2	1	–	110	7	70	57.5
MPsC	6	1	1	0.5	–	110	7	70	46.7
MPsD	6	1	1	0.5	–	110	10	100	50.5
MPsE	5	1	1	0.5	–	110	7	70	54.0
MPsF	5	1	1	0.5	–	110	10	100	53.9
NiM	5	1	1	0.5	0.45	110	10	100	63.0

airflow of 90 l/min.

To optimize particle deposition during aerosolization, the PS and the impaction cups of all stage were coated with a 1 % Tween 80 solution (v/v) in ethanol and allowed to dry completely prior to testing.

For each analysis, six methylcellulose capsules (size 3) were manually filled with 40 mg of each powder and aerosolized into the ACI for 5 s using a Bravo X Bio pump. After aerosolization, the deposited powder in each stage was retrieved with a known volume of water and absorbance intensities were measured at a wavelength of 540 nm. Aqueous microparticles dispersions in water at different concentration were used as standard. The same experimental procedure was repeated using NiM_{Sor}. In this case, the amount of drug deposited on each stage was quantified by HPLC analysis. Simultaneously, Rhodamine B fluorescence was measured from the same samples to trace the distribution of the microparticle matrix.

To characterize the aerodynamic performance of the formulations, several key parameters were calculated based on the deposition profile obtained from the ACI. These include the Emitted Fraction Percentage (EF%), which indicates the amount of powder released from the DPI relative to the total mass loaded into the capsules; the Inhaled Powder Percentage (IP%) that is the fraction of the emitted powder that effectively deposits along the various ACI stages; the Mass Median Aerodynamic Diameter (MMAD), which represents the aerodynamic diameter at which half of the particle mass consists of smaller particles and the other half of larger ones, determined from the cumulative deposition profile; the Geometric Standard Deviation (GSD) described the variability in particle size and is calculated by dividing the MMAD with the particle diameter at the 84.1 % point of the cumulative distribution curve. Finally, the Fine Particle Fraction (FPF%) represents the percentage of particles with an aerodynamic diameter smaller than 5 μm, reflecting their potential for deep lung penetration (Ahmed et al., 2025).

2.7.5. Rheological analysis

Rheological analyses were carried out on aqueous mucin dispersions (6 % w/v), both alone or in presence of NiM_{Sor} at concentrations of 2.5 and 10 mg/mL. Measurements were performed at 37 °C, immediately after preparation (T0) and after 3 h of incubation (T3), using a rotational rheometer (TA Instruments, New Castle, DE, USA) equipped with a 20 mm Peltier plate and a parallel flat plate, with a constant gap of 200 μm The linear viscoelastic region (LVR) of mucin was identified through a strain sweep test ranging from 0.01 % to 1 %. Following this, a flow sweep was performed on all samples with a shear rate of 10–100 1/s to measure the complex viscosity (η*). All rheological measurements were carried out in triplicate, and data acquisition and analysis were performed using the Trios v3.3 software from TA Instruments. As a control, the same procedure was applied to microparticles made only with mannitol (MAN_{micro}).

3. Results and discussion

In this paper, we describe the production and characterization of an inhalable Nano into Micro (NiM) formulation based on microparticles, named NiM_{Sor}, made by functional excipients and Sorafenib (Sor)-loaded polymeric nanoparticles, targeted to the folate receptor, for the local treatment of lung cancer. The schematic representation of the formulation production is described in Scheme 1.

In general, redistribution of an actively targeted nanoparticle to a lung tumor results from the interplay of administration route, physical–chemical nanoparticle properties, passive tumor accumulation (EPR) and active ligand-receptor interactions. The most effective approaches typically combine local pulmonary delivery or pharmacokinetic optimization (stealth coatings, appropriate size) with strategies that overcome microenvironmental barriers and protein corona effects (Al Khatib et al., 2023; Patton and Byron, 2007; Wang et al., 2024). Pulmonary delivery allows much higher local drug concentrations compared with intravenous injection, while also reducing systemic toxicity, although deposition strongly depends on particle size, aerodynamic behavior and clearance by alveolar macrophages. Active targeting ligands such as FA can be used to decorate the nanocarriers to enhance binding and uptake by lung tumor cells once the particles are deposited in the airways.

Recent studies highlight the potential of inhalable nanoparticles with active or local targeting strategies for lung cancer therapy. Gelatin nanoparticles functionalized with epidermal growth factor (EGF) and loaded with doxorubicin (EGNP–DOX) were administered by

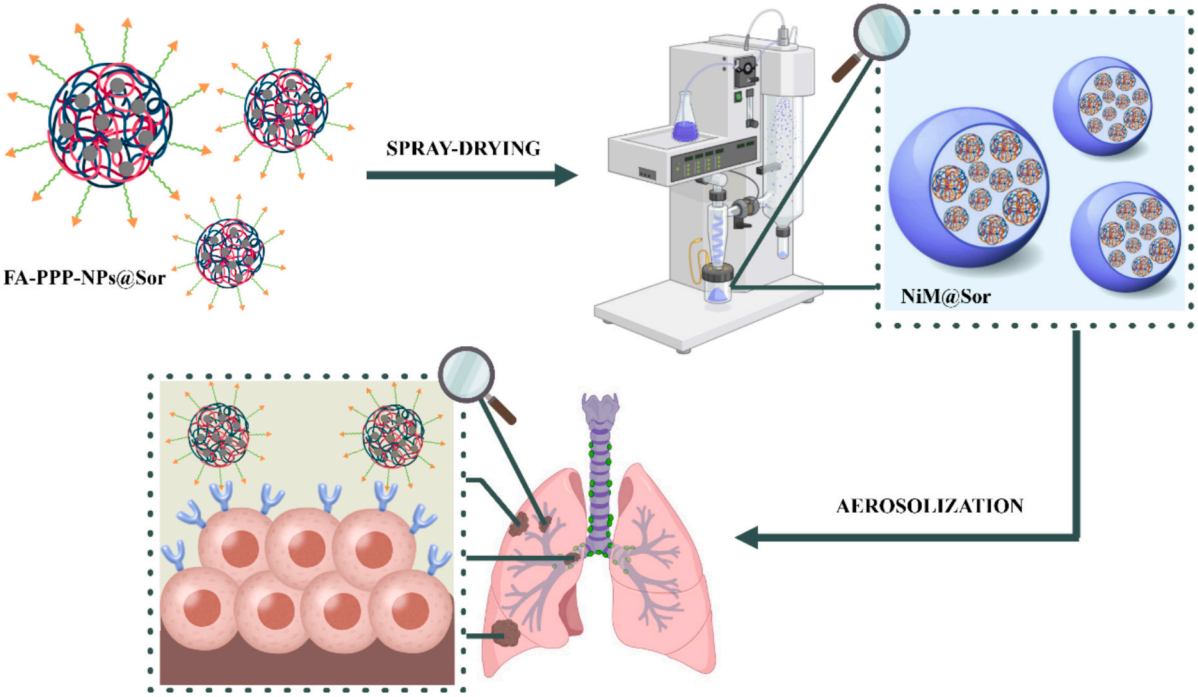

Scheme 1. Schematic representation of NiM_{Sor} production by the spray drying (SD) process.

nebulization in murine models of non-small cell lung cancer (NSCLC). These particles achieved selective uptake in EGFR-overexpressing cells, prolonged retention in the lungs for at least 24 h, and induced nearly 90 % tumor growth inhibition with 100 % survival of treated mice, while minimizing inflammatory responses (Long et al., 2014). More recently, afatinib-loaded PLGA nanoparticles optimized for inhalation showed favorable aerodynamic properties for deep lung deposition and strong cytotoxicity in KRAS-mutant NSCLC cell lines, suggesting their potential for localized therapy with reduced systemic exposure (Elbatanony et al., 2021). All these previous results indicate that inhalation, combined with molecular targeting strategies such as ligand functionalization, can significantly improve the therapeutic index of nanomedicines for lung cancer by maximizing local concentration, enhancing tumor selectivity, and minimizing systemic toxicity.

3.1. Synthesis and characterization of the PHEA-g-PLGA-g-PEG-FA

To obtain polymeric nanoparticles, a multifunctional copolymer was produced, capable of forming stable Sor-loaded polymeric nanoparticles in physiological media. The main polymer backbone, the α,β-poly(N-2-hydroxyethyl)-D,L-aspartamide (PHEA), was selected for its biocompatibility, which is crucial for pulmonary delivery, as well as its chemical versatility, as each repeating unit contains a reactive hydroxyl group that allows for easy functionalization (Di Meo et al., 2015; Triolo et al., 2017). Poly(lactic-*co*-glycolic acid) (PLGA) was grafted onto PHEA backbone, using a carbodiimide-mediated coupling reaction, to make the resulting PHEA-*g*-PLGA copolymer highly suitable for nanoparticle formation and enabling the encapsulation of hydrophobic drugs such as Sor.

To enhance mucus penetration and provide active targeting of cancer cells, the PHEA-*g*-PLGA was further functionalized with a folate derivative of polyethylene glycol (H_2N-PEG-FA). The derivatization of H_2N-PEG-NH_2 with FA was efficiently carried out through CDI-mediated activation and in a reaction time suitable for amide bond formation while minimizing possible side reactions. A two-step purification process enabled effective isolation of the H_2N-PEG-FA conjugate.

To obtain FA-surface decorated nanoparticles for improving active tumor cell targeting, H_2N-PEG-FA was linked to PHEA-*g*-PLGA, and the obtained folate copolymer used for the production of Sor-loaded nanoparticles (Iwakiri et al., 2008; Narmani et al., 2023).

The obtained copolymer PHEA-*g*-PLGA-*g*-PEG-FA was characterized by ^{1}H NMR spectroscopy, which allowed calculating the derivatization degree in PLGA and PEG-FA (DD_{PLGA} and $DD_{PEG\text{-}FA}$, respectively). In particular, the DD_{PLGA} was calculated by comparing the integral of the peaks related to protons at δ 1.5–1.9 assigned to PLGA with the integral of the peak related to the protons at to δ 3.5 assigned to PHEA backbone. The value was found to be equal to 3.3 ± 0.2 mol %, corresponding to about 6 molecules of PLGA/macromolecules. The $DD_{PEG\text{-}FA}$ was calculated by comparing the integral of the peaks related to protons at δ 3.7 assigned to PEG with the integral of the peak related to the protons at to δ 3.5 assigned to PHEA backbone, corresponding to about 8 molecules of PEG-FA/macromolecules. The absolute and relative $\bar{M}_w$ of PHEA-*g*-PLGA-*g*-PEG-FA, determined by SEC, were found to be equal to 193,230 Da ($\bar{M}_w/\bar{M}_n = 1.39$) and 110,987 Da ($\bar{M}_w/\bar{M}_n = 1.33$), respectively. The synthetic procedure of PHEA-*g*-PLGA-*g*-PEG-FA, graft copolymer is described in Fig. 1.

3.2. Production and characterization of PHEA-g-PLGA-g-PEG-FA nanoparticles (FA-PPP-NPs)

Once synthesized, the PHEA-*g*-PLGA-*g*-PEG-FA graft copolymer was used to obtain Sor-loaded polymeric nanoparticles using the nanoprecipitation method (Craparo et al., 2022b). This approach briefly allows the formation of stable nanoparticles in aqueous media, thanks to the physical–chemical properties of the synthesized polymer, which promotes the entrapment of Sor within the hydrophobic core during self-assembly, thereby improving its apparent solubility and potential bioavailability.

The formulation process demonstrated high efficiency, as evidenced by recovery yield of 83 wt% after freeze-drying. Drug loading (DL%) and encapsulation efficiency (EE%) of FA-PPP-NPs@Sor, determined by HPLC, were found to be 10 wt% and 77 wt%, respectively (Table 2). Empty nanoparticles (FA-PPP-NPs) were prepared in the absence of drug by following the previously described procedure.

As shown in Table 2, the FA-PPP-NPs@Sor sample exhibits an average diameter of approximately 100 nm, which was significantly higher than that of the empty FA-PPP-NPs. This increase in size, together with a lower polydispersity index (PDI = 0.14), suggests that the presence of Sor influences the nanoprecipitation process, promoting the formation of more uniform and colloidally stable nanoparticles. Moreover, the ζ-potential of Sor-loaded nanoparticles was −14.8 ± 4.6 mV, which is lower than that observed for empty nanoparticles (–23.1 ± 4.2 mV), indicating that drug entrapment could give a partial localization of Sor at the nanoparticle surface.

To investigate the ability of nanoparticles to retain the drug, an in vitro release study on the FA-PPP-NPs@Sor sample was performed using two different media: a mixture of simulated lung fluid (SLF4, pH 7.4), to replicate physiological pulmonary microenvironment, and citrate buffer (pH 5.5), to mimic tumor microenvironments (Marques et al., 2011). Both vehicles were added with foetal bovine serum (FBS) (50:50 v/v). The results, reported in Fig. 2, demonstrate that the drug was released from the nanoparticle in a controlled manner, without exhibiting a burst effect release. In fact, after 24 h of incubation, the cumulative drug release reached 8.4 wt% in SLF4 medium and 21.7 wt% in the citrate buffer medium. Therefore, a significantly higher release profile is observed under the simulate tumour microenvironment, that could be particularly advantageous to allow enhancement of drug therapeutic efficacy at the target site.

Given their design for pulmonary administration, it was essential to investigate the ability of FA-PPP-NPs@Sor to avoid undesirable interactions with the mucus layer of the respiratory tract. Efficient penetration through this barrier is a crucial requirement for nanocarriers intended for local lung delivery, as it enables them to diffuse through mucus and reach the underlying epithelial cells, which represent the biological target (Lai et al., 2009).

To assess the effectiveness of pegylation in reducing interactions between nanoparticles with mucin, the main component of the lung mucus, turbidimetric analysis was performed (Craparo et al., 2022a). Specifically, transmittance at 650 nm of aqueous dispersions containing both mucin and either empty or drug-loaded nanoparticles was monitored for over 3 h, using a mucin dispersion as a blank. For comparison, the same analysis was conducted using unpegylated nanoparticles obtained from PHEA-*g*-PLGA (PP-NPs sample). Data was expressed by plotting the ratio of the sample's transmittance to that of mucin blank as a function of incubation time. As showed in Fig. 3, the values of transmittance ratio for both FA-PPP-NPs@Sor and FA-PPP-NPs remained consistently close to 1, indicating negligible interaction with mucin. In contrast, the unpegylated PP-NPs exhibited a significantly reduced transmittance ratio, reflecting increased turbidity due to strong nanoparticle–mucin interactions, likely resulting from the absence of steric stabilization provided by PEG chains. Therefore, these nanoparticles showed suitable properties to be administered locally to the lung for anticancer therapy. These findings agree with previous studies demonstrating that surface pegylation reduces muco-adhesion by forming a hydrophilic, non-adhesive corona that limits non-specific interactions with mucus components (Craparo et al., 2024; Huckaby and Lai, 2018; Scialabba et al., 2024).

To evaluate the ability of Sor carried by targeted nanoparticles to selectively killing the tumor cells instead of healthy one, in vitro cytotoxicity of FA-PPP-NPs@Sor was assessed on both human lung cancer (A459) and healthy epithelial bronchial cells (16 HBE). The A549 cell

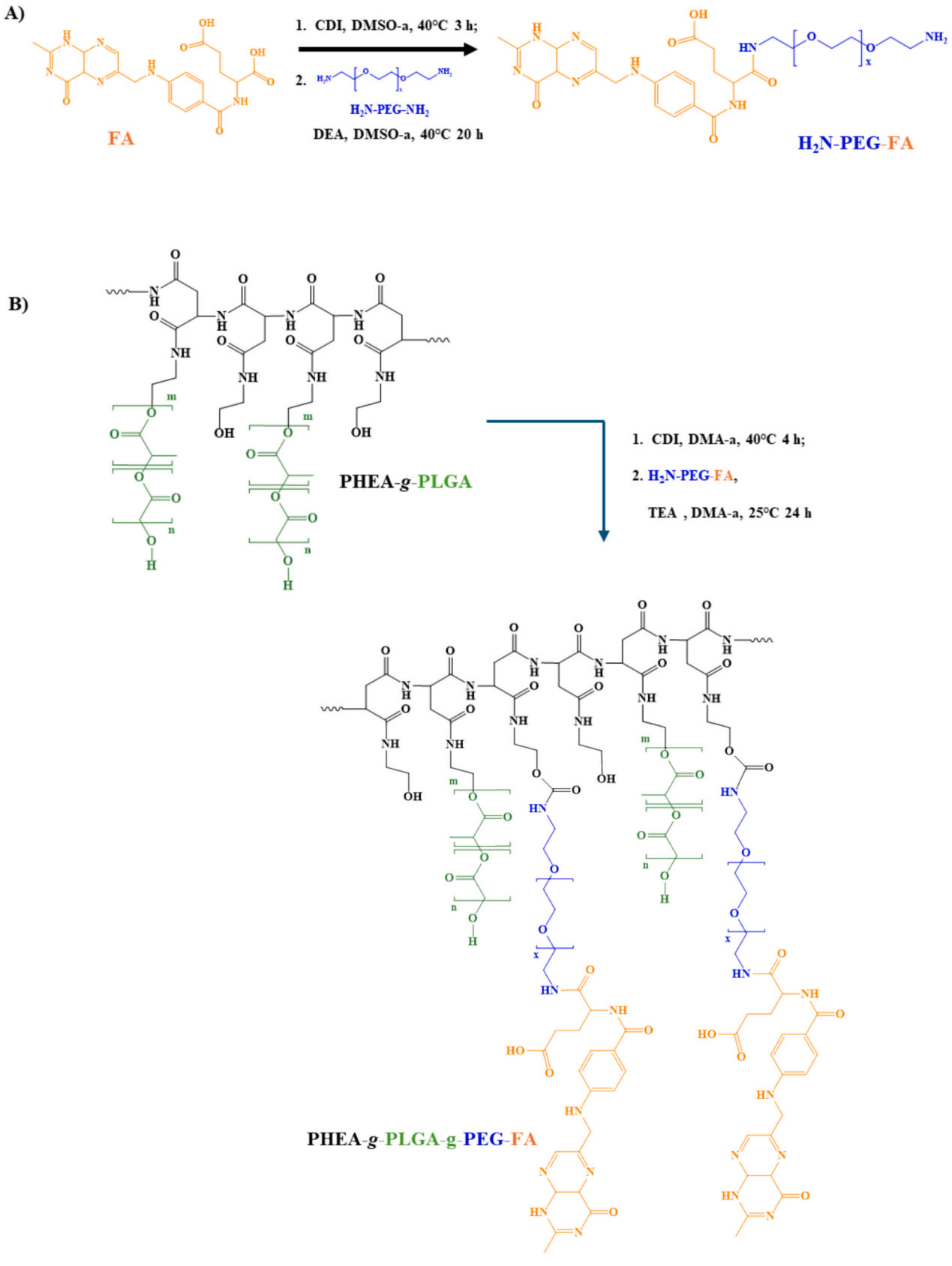

Fig. 1. Synthetic procedure of: (A) H_2N-PEG-FA and (B) PHEA-*g*-PLGA-*g*-PEG-FA (m = n = 92; x = 44).

Table 2
Mean Size ($Z_{Average}$), PDI, ς −potential, of empty FA-PPP-NPs and FA-PPP-NPs@Sor, in aqueous dispersion, and DL%, and EE% and yield % w/w after freeze-drying.

Sample	$Z_{Average}$ (nm)	PDI	ς −potential (mV)	DL %	EE %	Yield%
FA-PPP-NPs	55.92	0.29	−23.1 ± 4.6	–	–	83 ± 2.3
FA-PPP-NPs@Sor	109.2	0.14	−14.8 ± 4.2	10	77	71 ± 4.3

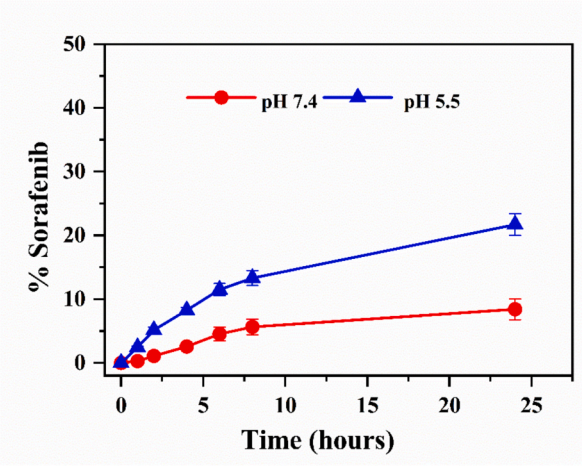

Fig. 2. Sorafenib release profile from the FA-PPP-NPs@Sor sample at pH 7.4 in simulated lung fluid (SLF4) (red) and at pH 5.5 in citrate buffer (blue) media at 37 °C, as a function of incubation time (n = 3).

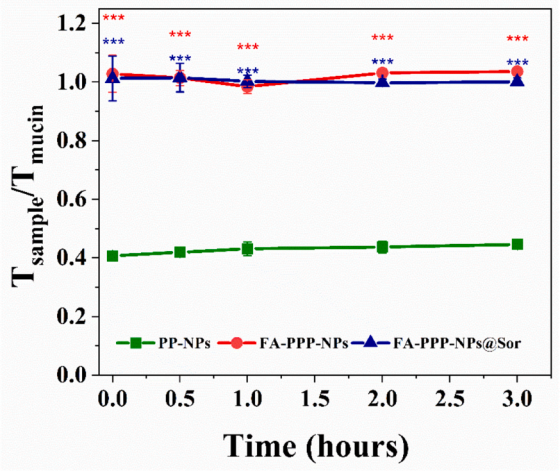

Fig. 3. Turbidimetric analysis of mucin dispersion (1 mg/mL) in the presence of FA-PPP-NPs, FA-PPP-NPs@Sor, and PP-NPs samples, as a function of the incubation time. Values are expressed as a ratio of the transmittance of the samples in mucin compared to the transmittance of samples in water. (***p < 0.005).

line was chosen as a model of cancer cells with folate receptor over-expression (Xia et al., 2018), whereas 16HBE cells serve as a model of healthy cells lacking this receptor (Licciardi et al., 2013; Zhang et al., 2016) In a first set of experiments, the cytocompatibility of the produced empty nanoparticles was assessed using an MTS assay on all selected cell lines. Cells were incubated with increasing concentrations of empty FA-PPP-NPs, ranging from 0.06 mg/mL to 0.6 mg/mL, for 24 and 48 h. The results, reported in Fig. 4A and 4B, indicated high cytocompatibility of empty nanoparticles under these tested conditions. Subsequent experiments, in which both 16HBE and A549 cells were incubated with Sor-loaded nanoparticles (FA-PPP-NPs@Sor), revealed a clear differential response. Obtained data are also reported in Fig. 4A and 4B.

Notably, the FA-targeted nanoparticles exhibited substantially lower cytotoxicity on 16HBE compared to free Sor (Fig. 4A). As reported in Table 3, the IC_{50} and maximum inhibition (I_{max}) for FA-PPP-NPs@Sor in 16HBE cells after 48 h of incubation were 69.0 ± 3.1 μM and 76.1 ± 2.6 %, respectively – both significantly improved in terms of safety relative to free Sor, which exhibited an IC_{50} of 17.7 ± 2.3 μM and an I_{max} of 96 ± 1.5 % after 48 h of incubation.

In contrast, A549 cancer cells demonstrated pronounced sensitivity to the FA-targeted nanoparticle formulation (Fig. 4B), with an IC_{50} of 18.0 ± 3.2 μM and an I_{max} of 95.2 ± 3.4 % after 48 h of incubation, indicating retained therapeutic efficacy. These values are consistent with those observed for free Sorafenib in A549 cells (IC_{50} = 8.0 ± 1.2 μM; I_{max} = 100 ± 1.5 %), confirming that the drug active targeting improve anticancer activity of Sor on cancer cells.

Overall, these results underscore the improved therapeutic index of Sor when entrapped into FA-PPP-NPs@Sor in tumour cells while significantly reducing the impact on non-tumorigenic cells, supporting its potential as a selective and safe strategy for targeted cancer therapy.

To further confirm that the selective cytotoxicity of the nanoparticle system toward cancer cells is mediated by folic acid targeting, an additional experiment was performed on A549 tumour cells. In detail, cells were pre-incubated with an excess of free FA for 24 h prior to treatment with the nanoparticle formulation, to competitively inhibit the folate receptor, thereby preventing receptor-mediated internalization of the FA-decorated nanoparticles (Fig. 4B). As expected, blocking the receptor significantly impaired the cytotoxic effect of FA-PPP-NPs@Sor. The IC_{50} increased to over 100 μM and the maximum inhibition dropped to 57.8 ± 1.4 % after 48 h of incubation, compared to data observed in untreated A549 cells (Table 3).

Therefore, the marked reduction in efficacy following receptor blockade confirms that the therapeutic action of the FA-PPP-NPs@Sor is strongly dependent on receptor-mediated targeting, highlighting the key role of FA in enhancing the selectivity and safety profile of the system.

To confirm that the FA-decorated nanoparticles are internalized due to the presence of the FA receptor on the cells, a cellular uptake assay was conducted and reported in Fig. 5; in particular, fluorescent nanoparticles (flu_FA-PPP-NPs@Sor) were produced starting from the rhodamine (RhB)-labelled PHEA-*g*-PLGA-*g*-PEG-FA graft copolymer, also in the presence of free FA and incubated with cells to evaluate the uptake (Fig. 5).

After 4 h of incubation, FA-functionalized samples were clearly internalized by A549 cells, as indicated by the red fluorescence signal. In contrast, the presence of free FA blocked cellular uptake of FA-targeted nanoparticles.

To investigate the anti-metastatic potential of FA-PPP-NPs@Sor nanoparticles in lung cancer, a wound healing assay was carried out on A549 cells. This assay is widely used to evaluate cell migration, a key process involved in tumor metastasis (Shukla et al., 2020). As illustrated in Fig. 6, a scratch was created on a confluent monolayer of A549 cell lines prior to treatment (time = 0), and cellular migration toward wound closure was monitored at 24 and 48 h post-treatment.

Wound healing was quantified by measuring the reduction in the scratch area following treatment with Sor and FA-PPP-NPs@Sor nanoparticles. At 24 h, both treatments resulted in a clear inhibition of cell migration compared to the control, with Sor showing a less wound closure than FA-PPP-NPs@Sor. However, after 48 h, a notable difference in cell migration was observed between the two treatments. Cells treated with Sor showed 40.2 % wound closure, whereas those treated with FA-PPP-NPs@Sor exhibited a significantly lower closure rate of 27.0 %, indicating a stronger inhibition of migration. These findings suggest that FA-PPP-NPs@Sor nanoparticles more effectively inhibit A549 cell migration over time compared to free Sorafenib, highlighting their enhanced potential in preventing lung cancer metastasis. This improved

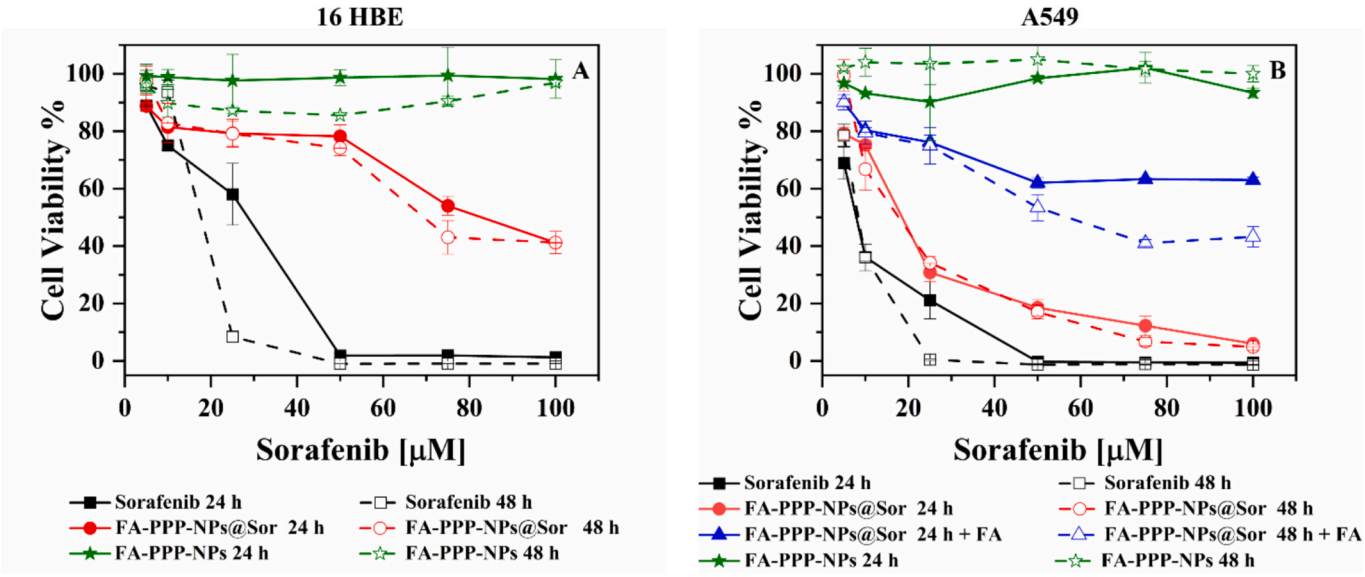

Fig. 4. In vitro cell viability and anticancer effect of 16 HBE (A) and A549 (B) treated with FA-PPP-NPs (green symbols), FA-PPP-NPs@Sor (red symbols) and Sor (black symbols) for 24 h (solid lines) and 48 h (dashed lines).

Table 3
Half maximal inhibitory concentration (IC_{50}) and maximum cell growth inhibition (I%) calculated for free Sor and FA-PPP-NP@Sor on 16 HBE and A549 cell lines.

Cell lines	Sample	$IC50^{24h}$ (μM)	I^{24h}_{max} (%)	$IC50^{48h}$ (μM)	I^{48h}_{max} (%)
16 HBE	Sor	29 ± 0.1	100 ± 1.2	17.7 ± 2.3	96 ± 1.5
	FA-PPP-NP@Sor	83 ± 1.2	59 ± 2.3	69.0 ± 3.1	76.1 ± 2.6
A549	Sor	8 ± 0.4	100 ± 0.8	8.0 ± 1.2	100 ± 1.5
	FA-PPP-NP@Sor	18 ± 0.3	94.1 ± 1.5	18.0 ± 32	95.2 ± 3.4
A549 + FA	FA-PPP-NP@Sor	>100	37 ± 24	56.4 ± 3.4	57.8 ± 1.4

ability is likely due to the controlled and prolonged release of Sor from the nanoparticle system, which maintains therapeutic levels of the drug over time and enhances its efficacy in limiting cell migration.

3.3. Production and characterization of inhalable Nano into Micro (NiM) particles

To obtain inhalable microparticles suitable for deposition of FA-PPP-NPs@Sor into the deep lung in the treatment of lung cancer, the Nano into Micro (NiM) strategy was employed. This involved encapsulating the drug-loaded nanoparticles into microparticles composed of functional excipients, such as mannitol (MAN), leucine (LEU) and N-acetyl cysteine (NAC), via spray drying (SD) (Craparo et al., 2024; Mancini et al., 2023). MAN was chosen as an osmotic agent to improve lung mucus hydration and increase its fluidity. NAC was included for its mucolytic properties, thanks to its thiol groups that help break down mucus (Mancini et al., 2023). However, NAC tends to reduce powder flowability and increase adhesiveness in spray-dried formulations. To overcome this, LEU was added to enhance powder dispersibility and aerosolization, improve emitted dose and fine particle fraction, and protect the particles from degradation caused by humidity . In the first step, the matrix formulation was optimized by varying the composition of the liquid feed in terms of MAN, LEU, and NAC concentrations. To further modulate the aerodynamic proprieties of the microparticles obtained, the porogen agent ammonium bicarbonate (AB) was also added to the liquid feed (Craparo et al., 2024). Upon spray drying, AB decomposes thermally into gaseous products (CO_2, NH_3, and H_2O), which generate internal porosity within the microparticles. This porosity can reduce particle density, enhancing aerosolization efficiency and improving deep lung deposition (Craparo et al., 2024). Additionally, 0.05 % w/v RhB was included in the formulation to allow fluorescence-based traceability. Several empty microparticles matrices were produced by systematically varying formulation parameters, including MAN concentrations (5–6 % w/v), NAC/LEU ratios (1:1 and 1:2), and porogen content (0.5 % and 1 % w/v). Spray drying process parameters such as pump and aspiration were also varied, while maintaining the liquid feed composition constant. Table 1 (experimental section) summarizes the w/v concentrations of each component in the liquid feed, the specific process parameters used, and the corresponding percentage yields obtained for each microparticle batch, which results above 45 wt % for all samples. Moreover, all the obtained microparticle samples were characterized through morphological analysis using a Scanning Electron Microscope (SEM), as shown in Fig. 7.

The SEM images revealed that microparticles exhibit a predominant spherical morphology. However, increased polydispersity and enhanced surface porosity were observed in the formulation in which 1 % w/v of AB was added in the liquid feed (samples MPsA and MPsB), in comparison to those prepared with 0.5 % w/v of AB. The particle size was calculated from SEM images to determine the geometric diameter (d_{geo}) of the microparticles. Additionally, the tapped density (ρ_{tapp}), bulk density (ρ_{bulck}), and Hausner index (HI) were calculated for each powder sample using the syringe method (Scialabba et al., 2024). Based on these parameters, the theoretical aerodynamic diameter (d_a) of each microparticle sample was calculated. A comprehensive summary of these results is provided in Table 4.

All the obtained microparticle formulations showed a theoretical aerodynamic diameter (d_a) below 5 μm, indicating their potentially suitability for deposition in the lower respiratory tract upon inhalation. Based on their favorable d_a and HI values, the microparticle samples named MPsE, and MPsF were selected for further evaluation of aerodynamic behavior using an Andersen Cascade Impactor (ACI) as described in the experimental section.

Fig. 8 shows the percentage distribution of powder deposition across the different stages of ACI. According to current regulatory guidelines and literature, inhalable dry powder formulations intended for deep lung delivery should typically exhibit MMAD values between 1–5 μm

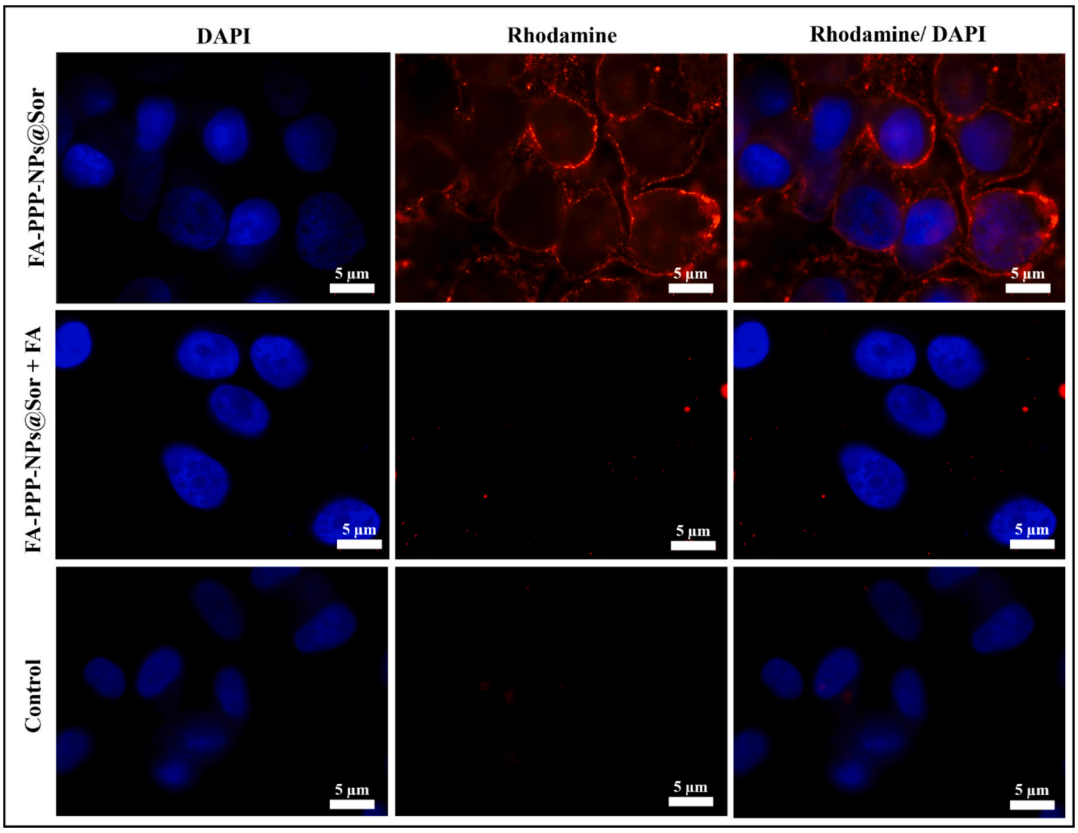

Fig. 5. Cell uptake study: fluorescence microscopy images of A549 cells after 4 hrs incubation with FA-PPP-NPs@Sor, without and in the presence of free FA, (bar represents 5 µm).

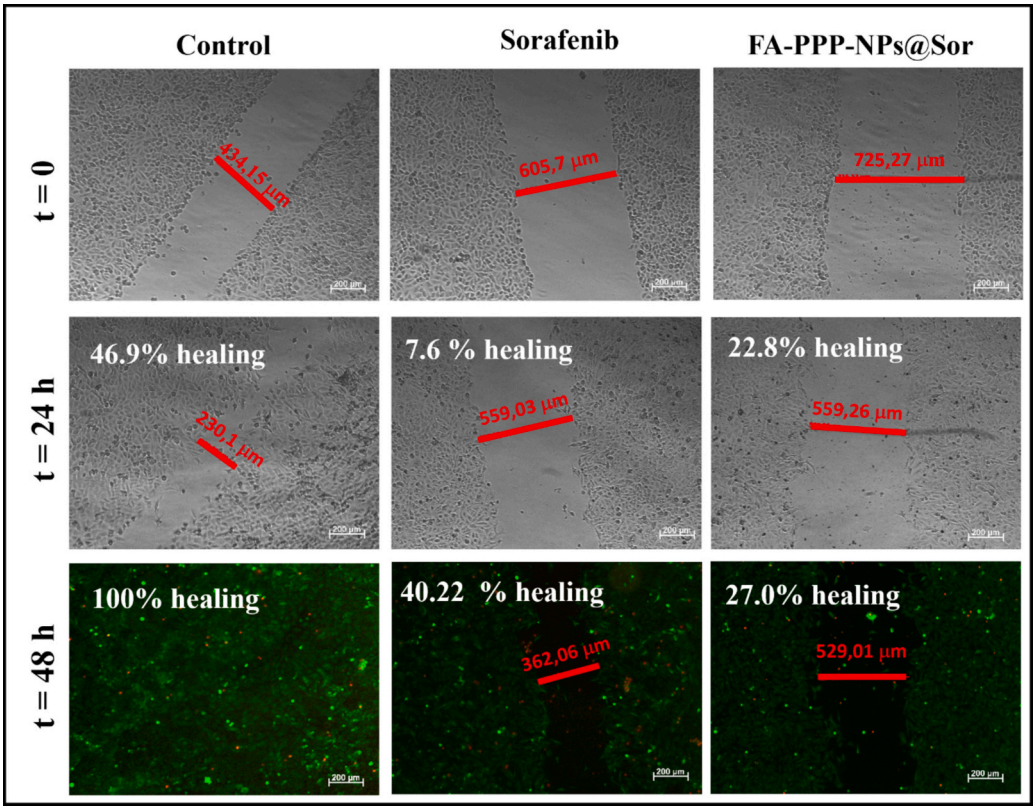

Fig. 6. Wound healing assay at Sorafenib concentration of 25 µM on A549 cell line by optical microscopy. Magnification 5X: scale bar 200 µm.

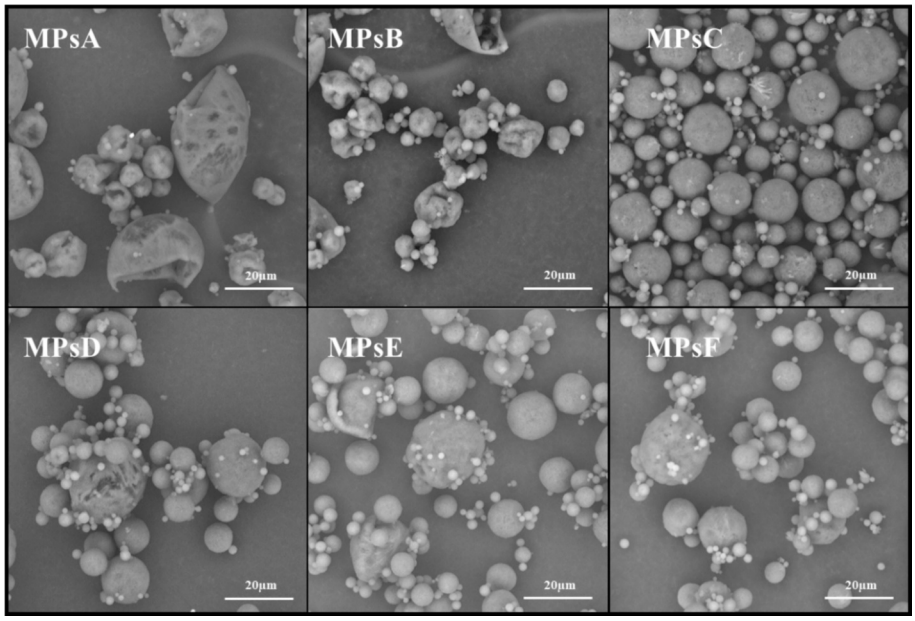

Fig. 7. SEM images of the empty microparticle samples.

Table 4
Bulk density (ρ_{bulk}) and tapped density (ρ_{tapped}), Hausner Index (HI), geometric diameter (d_{geo}) and aerodynamic diameter (d_a) of the obtained microparticle samples.

Sample	ρ_{bulk}	ρ_{tapped}	HI	d_{geo} (mm)	d_a (mm)
MPsA	0.23 ± 0.04	0.31 ± 0.02	1.31 ± 0.12	4.28 ± 3.44	2.90 ± 0.35
MPsB	0.26 ± 0.03	0.37 ± 0.03	1.41 ± 0.14	4.00 ± 2.33	2.43 ± 0.24
MPsC	0.30 ± 0.04	0.39 ± 0.04	1.28 ± 0.17	4.37 ± 2.38	2.72 ± 0.31
MPsD	0.33 ± 0.04	0.43 ± 0.06	1.30 ± 0.11	3.72 ± 2.92	2.45 ± 0.27
MPsE	0.35 ± 0.05	0.46 ± 0.05	1.31 ± 0.14	3.58 ± 2.60	2.43 ± 0.27
MPsF	0.34 ± 0.03	0.42 ± 0.04	1.24 ± 0.11	3.31 ± 2.25	2.15 ± 0.35
NiM_{Sor}	0.26 ± 0.03	0.34 ± 0.04	1.31 ± 0.19	1.84 ± 1.07	1.07 ± 0.18

and FPF% values above 30 % to ensure efficient deposition in the lower respiratory tract (Abdelaziz et al., 2018; Craparo et al., 2024). Among our samples, both MPsE and MPsF met these criteria, confirming their suitability as viable candidates for pulmonary drug delivery.

A more thorough comparison between MPsE and MPsF samples revealed that the MPsF formulation exhibited superior aerodynamic performance, with an MMAD of 3.6 μm and an FPF of 64.5 %, therefore it was selected for the development of Nano-in-Micro (NiM) systems incorporating PPP-FA-NPs@Sor (Craparo et al., 2024).

Specifically, a known quantity of FA-PPP-NPs@Sor (0.45 % w/v) was dispersed in the liquid feed, which was then processed under the same operating conditions and excipient composition used for the MPsF formulation, obtaining a Nim sample named NiM_{Sor}, with a final process yield of 63 wt% (Table 1). The improved yield may be attributed to the presence of nanoparticles, which may contribute to the formation of a more cohesive matrix during solvent evaporation, leading to more efficient particle recovery. Quantitative determination of DL% and EE% of NiM_{Sor} by HPLC resulted equal to 0.35 wt% and 100 wt%, respectively, an efficient Sor-loaded nanoparticle incorporation without drug loss during SD process.

Morphology analysis of the NIM_{Sor} sample by SEM (Fig. 9) revealed a

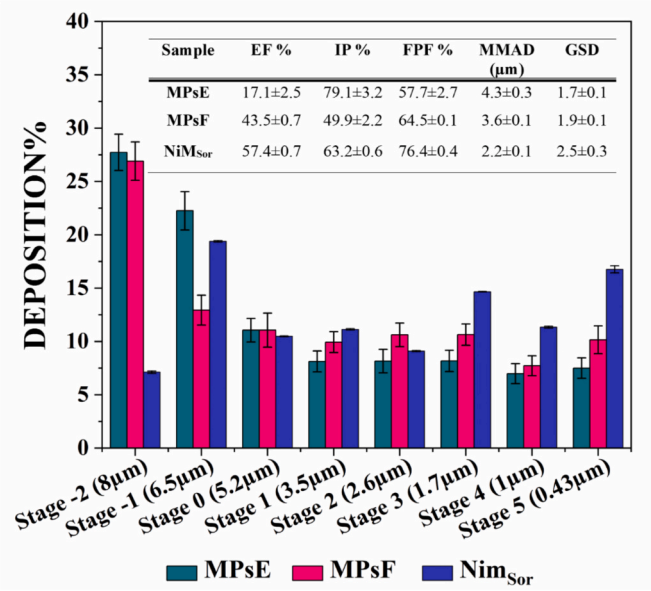

Fig. 8. Percentage of microparticle deposition (sample MpsE, MPsF and NiM_{Sor}) in the stages at different cut off by the Andersen Cascade impactor (ACI).

predominantly spherical shape, consistent with previous empty formulations. The particles exhibited a low PDI and good flowability, as also indicated by the derived bulk properties reported in Table 4.

Notably, the d_a of NiM_{Sor} was found to be lower than that of the empty microparticles, suggesting that the incorporation of the nanoparticles in the liquid feed affects the process of microparticle formation, acting as structuring agents during droplet drying, promoting a more compact and uniform particle morphology (Lintingre et al., 2016). This not only improves aerodynamic performance but may also contribute to enhanced deposition efficiency in the lower respiratory tract. Overall, these findings support the feasibility of the NiM_{Sor} formulation as a promising platform for pulmonary delivery of nanoparticle-based therapeutics, combining efficient drug encapsulation, and favourable aerodynamic properties for deep lung deposition.

To confirm the structural integrity of the NiM_{Sor} formulation and the

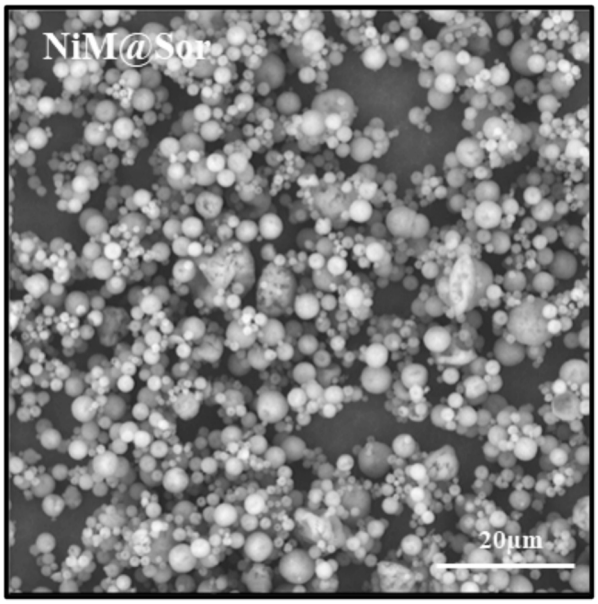

Fig. 9. SEM image of the NiM_{Sor} sample.

effective incorporation of nanoparticles within the microparticle matrix, a dual detection strategy was employed during aerodynamic evaluation. Specifically, both RhB, present in the microparticle matrix, and Sor, loaded within the FA-PPP-NPs, were quantified across the ACI stages. Data, reported in Fig. 8 as mean values, revealed a MMAD of 2.2 μm and FPF% of 76 % of the NiM_{Sor} are fully consistent with the size requirements for effective lower respiratory tract deposition, typically considered to be MMAD < 5 μm and FPF% > 50 % (Yang et al., 2008), with a narrow particle size distribution, supporting predictable and reproducible lung delivery.

Being the microparticle matrices made by water soluble excipients, the redispersion test of NiM_{Sor} microparticles in water showed that the obtained nanoparticle dispersion exhibited a Z-average, a polydispersity index and a ς potential values (reported in Table 5) that are fully comparable to those measured before the SD process. Moreover, after one year of storage at room temperature, the same redispersibility test showed results comparable to those obtained on the freshly prepared microparticle sample. These findings indicate that the SD process preserved the structural and colloidal integrity of the nanoparticles, without inducing significant aggregation or surface modification, even after a year of storage under conditions suitable for a pharmaceutical product.

To evaluate the effects of the dissolution of the functional excipients on pulmonary mucus, a rheological study was conducted in a 6 % w/v mucin dispersion, prepared following a previously validated experimental protocol (Scialabba et al., 2024). This mucin formulation is known to exhibit pseudoplastic behavior, characterized by a shear-thinning profile where viscosity decreases as shear rate increases, a rheological property like that observed in the sputum (Hazt et al., 2024; Wei et al., 2019). The study was performed by measuring the complex viscosity (η^*) of the mucin dispersion in the presence of NiM_{Sor} (2, 5, and 10 mg/mL) after two incubation times (T0 and T3) to assess whether the system's ability to modify the viscoelastic properties of the mucin dispersion. Moreover, to evaluate whether NAC is the component of the matrix composition that could affect the η^*, the analysis was also performed on Man-based microparticles (MAN_{micro}). The results reported in Fig. 10 demonstrate that the presence of NiM_{Sor} sample gives a significant mucus thinning effect than that obtained with MAN_{micro} sample, being the η^* of mucin dispersion incubated with NiM_{Sor} at t0 significantly reduced than that treated with MAN_{micro}, which maintained a viscosity like untreated mucin. At t3, the difference between the mucin samples incubated with MAN_{micro} and those exposed to NiM_{Sor} became even more pronounced, highlighting a time dependence of this effect.

Notably, the effect of NiM_{Sor} was also concentration-dependent, as a progressive reduction in viscosity was observed as the concentration of NiM_{Sor} (and consequently of NaC) increased in the mucin dispersion.

Taken together, these results provide compelling evidence of the mucoacting properties of the NiM_{Sor} formulations, which were able to significantly reduce the η^* of mucin dispersions in a time- and concentration-dependent manner. The pronounced thinning effect observed immediately after incubation and its further enhancement at prolonged contact time suggest a sustained interaction with the mucus matrix, likely attributable to the presence of NAC within the formulation. In contrast, the MAN_{micro} control microparticles, lacking NAC, did not significantly alter mucin rheology, reinforcing the hypothesis that NAC is the key functional component responsible for the observed viscoelastic changes. These findings support the potential of NiM_{Sor} as a promising inhalable carrier capable of overcoming the mucus barrier by modulating its viscoelastic properties, thereby facilitating deeper and more uniform drug-loaded carriers' penetration within the pulmonary environment.

Table 5
Mean Size ($Z_{Average}$), PDI, ς −potential values of freshly prepared NiM_{Sor} particles and after 1 year of storage at r.t., after redispersion in water.

Sample	$Z_{Average}$ (nm)	PDI	ς −potential (mV)
Freshly prepared	105.2	0.27	−8.59 ± 6.8
After 1 year storage	172.4	0.32	−13.2 ± 4.5

4. Conclusions

In this study, we successfully developed and characterized Sorafenib (Sor)-loaded mucus-penetrating nanoparticles (FA-PPP-NPs@Sor) for the local treatment of lung cancer. These nanoparticles were produced starting from a multifunctional graft copolymer based on α,β-poly(N-2-hydroxyethyl)-D,L-aspartamide (PHEA), chemically functionalized with poly(lactic-co-glycolic acid) (PLGA) to enable encapsulation of the hydrophobic drug and with folate-conjugated polyethylene glycol (PEG-FA) to enhance mucus penetration and actively target cancer cells overexpressing folate receptor. The resulting nanoparticles exhibited high drug loading and controlled release profile. The surface pegylation ensured minimal interaction with mucin, facilitating deeper penetration into the lung mucus barrier and efficient drug delivery to tumor cells.

The in vitro biological evaluation of FA-PPP-NPs@Sor demonstrated selective cytotoxicity towards lung cancer cells (A549), while maintaining a favorable safety profile in non-cancerous bronchial epithelial cells (16HBE). The nanoparticles significantly reduced A549 cell viability in a dose- and time-dependent manner, and competitive binding experiments confirmed folate receptor-mediated uptake. Moreover, cell uptake studies revealed that the carrier is internalized by the cells thanks to the FA surface decoration, and wound healing assays revealed a strong inhibition of cancer cell migration upon treatment with FA-PPP-NPs@Sor, suggesting their potential to impair metastatic behavior.

To improve pulmonary administration, these nanoparticles were further incorporated into inhalable Nano-into-Micro (NiM) systems using spray drying (SD). The resulting microparticles exhibited favorable aerodynamic properties, including a mass median aerodynamic diameter (MMAD) within the optimal range for deep lung deposition, stability under 1 year storage, giving the reconstitution of the nanoparticle dispersion. Furthermore, rheological studies indicated that NiM_{Sor} formulations significantly reduced mucus viscosity, mainly due to the presence of NaC into the matrix composition, enhancing nanoparticle dispersion into the lung fluids.

Therefore, inhalation of NiM_{Sor}, combined with FA active targeting ligand decoration of nanoparticles, highlights the potential of the formulation as an innovative and efficient drug delivery system for lung

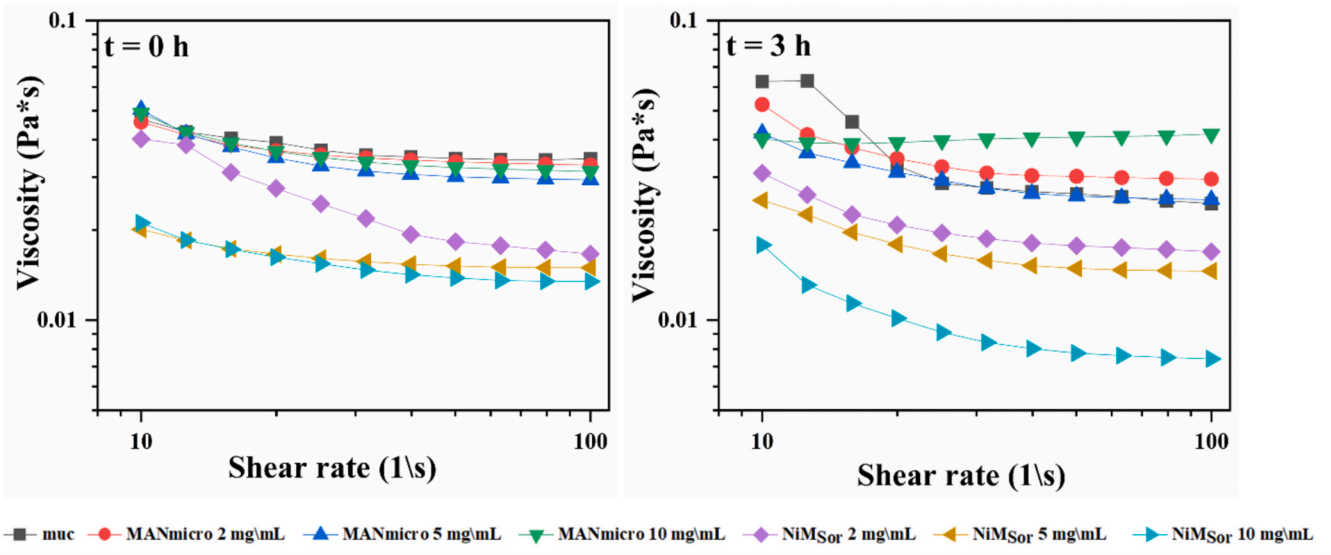

Fig. 10. Rheological trend of Mucin 6%, MAN_{micro} and NiM_{Sor}.

cancer therapy, and offers a dual advantage: high local concentration due to direct delivery of NiM particles to the lung, and improved selectivity to tumor cells of FA-decorated nanoparticles due to ligand-receptor recognition. At the same time, challenges remain, such as uneven particle distribution in the lung and the risk that protein adsorption in the pulmonary environment may mask targeting ligands.

CRediT authorship contribution statement

Cinzia Scialabba: Writing – original draft, Investigation, Formal analysis, Data curation, Conceptualization. **Federico Corsaro:** Formal analysis. **Salvatore Emanuele Drago:** Methodology, Data curation. **Emanuela Fabiola Craparo:** Writing – review & editing, Supervision, Data curation, Conceptualization. **Gennara Cavallaro:** Supervision, Project administration, Funding acquisition, Conceptualization.

Declaration of competing interest

The authors declare that they have no known competing financial interests or personal relationships that could have appeared to influence the work reported in this paper.

Acknowledgments

The authors thank ATeNCenter of University of Palermo – Laboratory of Preparation and Analysis of Biomaterials for analysis instruments, Mr. Francesco Paolo Bonomo for technical support.

Data availability

Data will be made available on request.

References

Abdelaziz, H.M., Gaber, M., Abd-Elwakil, M.M., Mabrouk, M.T., Elgohary, M.M., Kamel, N.M., Kabary, D.M., Freag, M.S., Samaha, M.W., Mortada, S.M., Elkhodairy, K.A., Fang, J.-Y., Elzoghby, A.O., 2018. Inhalable particulate drug delivery systems for lung cancer therapy: Nanoparticles, microparticles, nanocomposites and nanoaggregates. J. Control. Release 269, 374–392. https://doi.org/10.1016/j.jconrel.2017.11.036.

Abdellatif, A.A.H., Ali, A.T., Bouazzaoui, A., Alsharidah, M., Al Rugaie, O., Tolba, N.S., 2022. Formulation of polymeric nanoparticles loaded sorafenib; evaluation of cytotoxicity, molecular evaluation, and gene expression studies in lung and breast cancer cell lines. Nanotechnol. Rev. 11, 987–1004. https://doi.org/10.1515/ntrev-2022-0058.

Ahmed, R., Tewes, F., Aucamp, M., Dube, A., 2025. Formulation and clinical translation of inhalable nanomedicines for the treatment and prevention of pulmonary infectious diseases. Drug Deliv. Transl. Res. https://doi.org/10.1007/s13346-025-01861-5.

Al Khatib, A.O., El-Tanani, M., Al-Obaidi, H., 2023. Inhaled Medicines for Targeting Non-Small Cell Lung Cancer. Pharmaceutics. https://doi.org/10.3390/pharmaceutics15122777.

Blumenschein, G.R., Gatzemeier, U., Fossella, F., Stewart, D.J., Cupit, L., Cihon, F., O'Leary, J., Reck, M., 2009. Phase II, Multicenter, Uncontrolled Trial of Single-Agent Sorafenib in patients with Relapsed or Refractory, Advanced Non–Small-Cell Lung Cancer. J. Clin. Oncol. 27, 4274–4280. https://doi.org/10.1200/JCO.2009.22.0541.

Craparo, E.F., Cabibbo, M., Scialabba, C., Casula, L., Lai, F., Cavallaro, G., 2024. Rapamycin-based inhaled therapy for potential treatment of COPD-related inflammation: production and characterization of aerosolizable nano into micro (NiM) particles. Biomater. Sci. 12, 387–401. https://doi.org/10.1039/D3BM01210G.

Craparo, E.F., Cabibbo, M., Scialabba, C., Giammona, G., Cavallaro, G., 2022a. Inhalable Formulation based on Lipid-Polymer Hybrid Nanoparticles for the Macrophage Targeted delivery of Roflumilast. Biomacromolecules 23, 3439–3451. https://doi.org/10.1021/acs.biomac.2c00576.

Craparo, E.F., Drago, S.E., Quaglia, F., Ungaro, F., Cavallaro, G., 2022b. Development of a novel rapamycin loaded nano- into micro-formulation for treatment of lung inflammation. Drug Deliv. Transl. Res. 12, 1859–1872. https://doi.org/10.1007/s13346-021-01102-5.

Craparo, E.F., Sardo, C., Serio, R., Zizzo, M.G., Bondì, M.L., Giammona, G., Cavallaro, G., 2014. Galactosylated polymeric carriers for liver targeting of sorafenib. Int. J. Pharm. 466, 172–180. https://doi.org/10.1016/j.ijpharm.2014.02.047.

Di Meo, C., Cilurzo, F., Licciardi, M., Scialabba, C., Sabia, R., Paolino, D., Capitani, D., Fresta, M., Giammona, G., Villani, C., Matricardi, P., 2015. Polyaspartamide-Doxorubicin Conjugate as potential Prodrug for Anticancer Therapy. Pharm. Res. 32. https://doi.org/10.1007/s11095-014-1557-2.

Duruisseaux, M., Esteller, M., 2018. Lung cancer epigenetics: from knowledge to applications. Semin. Cancer Biol. 51, 116–128. https://doi.org/10.1016/j.semcancer.2017.09.005.

Elbatanony, R.S., Parvathaneni, V., Kulkarni, N.S., Shukla, S.K., Chauhan, G., Kunda, N. K., Gupta, V., 2021. Afatinib-loaded inhalable PLGA nanoparticles for localized therapy of non-small cell lung cancer (NSCLC)—development and in-vitro efficacy. Drug Deliv. Transl. Res. 11, 927–943. https://doi.org/10.1007/s13346-020-00802-8.

Hazt, B., Read, D.J., Harlen, O.G., Poon, W.C.K., O'Connell, A., Sarkar, A., 2024. Mucoadhesion across scales: Towards the design of protein-based adhesives. Adv. Colloid Interface Sci. 334, 103322. https://doi.org/10.1016/j.cis.2024.103322.

Hendrixson, M., Gladkiy, Y., Thyagarajan, A., Sahu, R.P., 2024. Efficacy of Sorafenib-based Therapies for Non-Small Cell Lung Cancer. Medical Sciences 12, 20. https://doi.org/10.3390/medsci12020020.

Huckaby, J.T., Lai, S.K., 2018. PEGylation for enhancing nanoparticle diffusion in mucus. Adv. Drug Deliv. Rev. 124, 125–139. https://doi.org/10.1016/j.addr.2017.08.010.

Iwakiri, S., Sonobe, M., Nagai, S., Hirata, T., Wada, H., Miyahara, R., 2008. Expression Status of Folate Receptor α is significantly Correlated with Prognosis in Non-Small-Cell Lung Cancers. Ann. Surg. Oncol. 15, 889–899. https://doi.org/10.1245/s10434-007-9755-3.

Kim, I., Byeon, H.J., Kim, T.H., Lee, E.S., Oh, K.T., Shin, B.S., Lee, K.C., Youn, Y.S., 2012. Doxorubicin-loaded highly porous large PLGA microparticles as a sustained- release inhalation system for the treatment of metastatic lung cancer. Biomaterials 33, 5574–5583. https://doi.org/10.1016/j.biomaterials.2012.04.018.

Kutkowska, J., Strzadala, L., Rapak, A., 2017. Synergistic activity of sorafenib and betulinic acid against clonogenic activity of non-small cell lung cancer cells. Cancer Sci. 108, 2265–2272. https://doi.org/10.1111/cas.13386.

Lababidi, N., Montefusco-Pereira, C.V., de Souza Carvalho-Wodarz, C., Lehr, C.-M., Schneider, M., 2020. Spray-dried multidrug particles for pulmonary co-delivery of antibiotics with N-acetylcysteine and curcumin-loaded PLGA-nanoparticles. Eur. J. Pharm. Biopharm. 157, 200–210. https://doi.org/10.1016/j.ejpb.2020.10.010.

Lai, S.K., Wang, Y.-Y., Hanes, J., 2009. Mucus-penetrating nanoparticles for drug and gene delivery to mucosal tissues. Adv. Drug Deliv. Rev. 61, 158–171. https://doi.org/10.1016/j.addr.2008.11.002.

Licciardi, M., Scialabba, C., Cavallaro, G., Sangregorio, C., Fantechi, E., Giammona, G., 2013. Cell uptake enhancement of folate targeted polymer coated magnetic nanoparticles. J. Biomed. Nanotechnol. 9. https://doi.org/10.1166/jbn.2013.1606.

Lintingre, E., Lequeux, F., Talini, L., Tsapis, N., 2016. Control of particle morphology in the spray drying of colloidal suspensions. Soft Matter 12, 7435–7444. https://doi.org/10.1039/C6SM01314G.

Long, J.T., Cheang, T. yun, Zhuo, S.Y., Zeng, R.F., Dai, Q.S., Li, H.P., Fang, S., 2014. Anticancer drug-loaded multifunctional nanoparticles to enhance the chemotherapeutic efficacy in lung cancer metastasis. J Nanobiotechnology 12. doi: 10.1186/s12951-014-0037-5.

Mancini, L., Paolantoni, M., Schoubben, A., Ricci, M., 2023. Development of spray-dried N-acetylcysteine dry powder for inhalation. Int. J. Pharm. 631, 122550. https://doi.org/10.1016/j.ijpharm.2022.122550.

Marques, M.R.C., Loebenberg, R., Almukainzi, M., 2011. Simulated Biological Fluids with possible Application in Dissolution Testing. Dissolut. Technol. 18, 15–28. https://doi.org/10.14227/DT180311P15.

Naccache, J.-M., Gibiot, Q., Monnet, I., Antoine, M., Wislez, M., Chouaid, C., Cadranel, J., 2018. Lung cancer and interstitial lung disease: a literature review. J. Thorac. Dis. 10, 3829–3844. https://doi.org/10.21037/jtd.2018.05.75.

Narmani, A., Ganji, S., Amirishoar, M., Jahedi, R., Kharazmi, M.S., Jafari, S.M., 2023. Smart chitosan-PLGA nanocarriers functionalized with surface folic acid ligands against lung cancer cells. Int. J. Biol. Macromol. 245, 125554. https://doi.org/10.1016/j.ijbiomac.2023.125554.

Patton, J.S., Byron, P.R., 2007. Inhaling medicines: Delivering drugs to the body through the lungs. Nat. Rev. Drug Discov. https://doi.org/10.1038/nrd2153.

Puleio, R., Licciardi, M., Varvarà, P., Scialabba, C., Cassata, G., Cicero, L., Cavallaro, G., Giammona, G., 2020. Effect of actively targeted copolymer coating on solid tumors eradication by gold nanorods-induced hyperthermia. Int. J. Pharm. 587, 119641. https://doi.org/10.1016/j.ijpharm.2020.119641.

Scialabba, C., Craparo, E.F., Cabibbo, M., Emanuele Drago, S., Cavallaro, G., 2024. Exploiting inhalable microparticles incorporating hybrid polymer-lipid nanoparticles loaded with Iloprost manages lung hyper-inflammation. Int. J. Pharm. 666, 124813. https://doi.org/10.1016/j.ijpharm.2024.124813.

Shukla, S.K., Kulkarni, N.S., Farrales, P., Kanabar, D.D., Parvathaneni, V., Kunda, N.K., Muth, A., Gupta, V., 2020. Sorafenib Loaded Inhalable Polymeric Nanocarriers against Non-Small Cell Lung Cancer. Pharm. Res. 37, 67. https://doi.org/10.1007/s11095-020-02790-3.

Su, Y., Wang, K., Li, Y., Song, W., Xin, Y., Zhao, W., Tian, J., Ren, L., Lu, L., 2018. Sorafenib-Loaded Polymeric Micelles As Passive Targeting Therapeutic Agents for Hepatocellular Carcinoma Therapy. Nanomedicine 13, 1009–1023. https://doi.org/10.2217/nnm-2018-0046.

Sung, H., Ferlay, J., Siegel, R.L., Laversanne, M., Soerjomataram, I., Jemal, A., Bray, F., 2021. Global Cancer Statistics 2020: GLOBOCAN estimates of Incidence and Mortality Worldwide for 36 Cancers in 185 Countries. CA Cancer J. Clin. 71, 209–249. https://doi.org/10.3322/caac.21660.

Takezawa, K., Okamoto, I., Yonesaka, K., Hatashita, E., Yamada, Y., Fukuoka, M., Nakagawa, K., 2009. Sorafenib Inhibits Non–Small Cell Lung Cancer Cell Growth by Targeting B-RAF in *KRAS* Wild-Type Cells and C-RAF in *KRAS* Mutant Cells. Cancer Res. 69, 6515–6521. https://doi.org/10.1158/0008-5472.CAN-09-1076.

Triolo, D., Craparo, E.F., Porsio, B., Fiorica, C., Giammona, G., Cavallaro, G., 2017. Polymeric drug delivery micelle-like nanocarriers for pulmonary administration of beclomethasone dipropionate. Colloids Surf. B Biointerfaces 151, 206–214. https://doi.org/10.1016/j.colsurfb.2016.11.025.

Wang, J., Ma, S., Chen, X., Zhang, S., Wang, Z., Mei, Q., 2019. The novel PI3K inhibitor S1 synergizes with sorafenib in non-small cell lung cancer cells involving the Akt-S6 signaling. Invest. New Drugs 37, 828–836. https://doi.org/10.1007/s10637-018-0698-2.

Wang, W., Hao, Y., Liu, Y., Li, R., Huang, D., Pan, Y., 2021. Nanomedicine in lung cancer: current states of overcoming drug resistance and improving cancer immunotherapy. WIREs Nanomed. Nanobiotechnol. 13. https://doi.org/10.1002/wnan.1654.

Wang, W., Zhong, Z., Huang, Z., Hiew, T.N., Huang, Y., Wu, C., Pan, X., 2024. Nanomedicines for targeted pulmonary delivery: receptor-mediated strategy and alternatives. Nanoscale. https://doi.org/10.1039/d3nr05487j.

Wei, L., Zhao, J., Bao, J., Ma, Y., Shang, Y., Gao, Z., 2019. The characteristics and clinical significance of mucin levels in bronchoalveolar lavage fluid of patients with interstitial lung disease. J. Invest. Med. 67, 761–766. https://doi.org/10.1136/jim-2018-000785.

Xia, J.-M., Wei, X., Chen, X.-W., Shu, Y., Wang, J.-H., 2018. Folic acid modified copper nanoclusters for fluorescent imaging of cancer cells with over-expressed folate receptor. Microchim. Acta 185, 205. https://doi.org/10.1007/s00604-018-2743-4.

Yang, W., Peters, J.I., Williams, R.O., 2008. Inhaled nanoparticles—A current review. Int. J. Pharm. 356, 239–247. https://doi.org/10.1016/j.ijpharm.2008.02.011.

Zhang, J., Gold, K.A., Kim, E., 2012. Sorafenib in non-small cell lung cancer. Expert Opin. Invest. Drugs 21, 1417–1426. https://doi.org/10.1517/13543784.2012.699039.

Zhang, M., Kim, Y.-K., Cui, P., Zhang, J., Qiao, J., He, Y., Lyu, J., Luo, C., Xing, L., Jiang, H., 2016. Folate-conjugated polyspermine for lung cancer–targeted gene therapy. Acta Pharm. Sin. B 6, 336–343. https://doi.org/10.1016/j.apsb.2016.03.010.